Dynamical modeling of non-proportionally damped multibody systems using a modal Udwadia–Kalaba formulation based on complex modes of the dissipative subsystems

François Fabre, Jean-Loïc Le Carrou, Baptiste Chomette

Dynamical modeling of non-proportionally damped multibody systems using a modal Udwadia-Kalaba formulation based on complex modes of the dissipative subsystems

François Fabre[a], Jean-Loïc Le Carrou[a,*], Baptiste Chomette[b]

[a]*Sorbonne Université, CNRS, Institut Jean Le Rond d'Alembert, Équipe Lutheries-Acoustique-Musique, F-75005 Paris, France*
[b]*Ecole Centrale de Lyon, CNRS, ENTPE, LTDS, UMR5513, 69130 Ecully, France*

Abstract

This paper presents a modal Udwadia-Kalaba formulation based on complex modal analysis. This alternative formulation is developed in the general case of vibro-acoustic systems with an internal cavity. In a similar manner to the original formulation, the global response of a constrained multibody system is expressed as a sum of its unconstrained response and a corrective term allowing the enforcement of constraints. The use of complex modes of the dissipative substructures has the advantage of leading to a set of ordinary differential equations, regarding the unconstrained response, even in the case of non-classically damped substructures. Moreover, in the frame of experimental substructuring, the estimation of complex modal parameters of a state-space representation is more straightforward than for real ones of the equivalent second order model, hence this alternative formulation is of prac-

*corresponding author
Email address: jean-loic.le_carrou@sorbonne-universite.fr (Jean-Loïc Le Carrou)

tical interest in this context. An academic example with non-proportional damping allows to validate the proposed modal formulation. Then two experimentally identified models of a guitar and a harp from Central Africa are coupled to a stiff string whose modal parameters are known from the analytic theory. The guitar model contains an acoustic degree of freedom and allows to illustrate the suitability of the Udwadia-Kalaba formulation to model coupled vibro-acoustic substructures. The harp model includes highly complex modes which allows to highlight the advantage of expressing the coupled response of the global system in terms of its complex modal coordinates.
Keywords: Udwadia-Kalaba, Substructuring, Internal vibro-acoustics, Non-proportional damping, Complex modes

1. Introduction

When performing the dynamical analysis of a structure, it may necessary to split it into substructures whose behavior is easier to characterize. Such situations might arise for example, in experimental configuration, when the complete structure is too large to be analyzed as a whole, or in a numerical case, when the number of degrees of freedom (dofs) leads to unreasonable computation time. This approach of splitting the problem into subparts is known as dynamic substructuring. When the global analysis presents no particular difficulty, dynamic substructuring may still be advantageous to conduct a parametric study componentwise or to build hybrid assemblies combining (discrete or continuous/analytical) model(s) and experimentally identified parts.

Constrained multibody systems have been studied for many years and

multiple methods were developed to deal with rigid bodies until recent decades. In the last 60 years, efforts have been put to take into account the elastic behavior of substructures thus further increasing the list of available formulations. de Klerk et al. [1] proposed a classification of these formulations in a general framework in which the structural dynamics are analyzed in three distinct domains: the physical, modal and frequency domains.

The physical domain includes the well known finite element method and others originally developed for rigid substructures, whose review was proposed by Lalausa and Bachau [2], such as Maggi's method [3, 4] and the Udwadia-Kalaba [5–9] (U-K) formulation. These methods require the knowledge of physical mass, stiffness and damping matrices for each substructure. In the frame of experimental substructuring, identification techniques [10] allow to estimate physical matrices but the damping matrix remains delicate to obtain, due to its high sensitivity to noise and inconsistencies in the data, making physical domain formulations unpractical.

On the other hand, frequency based substructuring (FBS) does not rely on the separate knowledge of mass, stiffness and damping properties. Instead, the dynamic behavior of the substructures is described by transfer functions which presents no particular difficulty to measure. Typical FBS methods are the admittance coupling [11, 12], the impedance coupling [13] and the Lagrange multipliers FBS (LM-FBS) coupling[14, 15]. Obviously, in order to transform the equations of motion from the time domain to the frequency domain, each substructure needs to be linear time invariant (LTI) and in steady-state which limits the case of applications.

Another option lies in the class of modal domain formulations, known

as component-mode synthesis (CMS). Although the use of CMS is not as straight forward as FBS for experimental substructuring, since it requires to perform modal analysis (and induces truncation effects due to the order reduction), it remains a useful solution for analyzing non-LTI multibody systems. Methods based on all kinds of structural modes have been proposed during the last 60 years to which an overview was given by Craig [16]. The most widespread CMS formulations are the Craig-Brampton [17] (combination of constraint modes and fixed-interface normal modes), MacNeal [18] and Rubin [19] (combination of attachment modes and free-interface normal modes) methods. In the last decade, with a view to modeling musical instruments as constrained multibody systems, Antunes and Debut [20] adapted the U-K formalism to continuous flexible systems using free-interface normal modes. The (modal) U-K formulation offers a compact and general solution (allowing for redundant and non-ideal constraints). The relevance of this new CMS method has been illustrated in several research works involving geometrical string non-linearities [21–23] and intermittent contacts [24].

Other promising approaches, developed for substructure-based system identification, constitute the class labeled state-space substructuring (SSS) which consists in assembling state-space models of substructures. Proposed in recent years, they can be linked to the physical or modal domain depending on the choice of state variables. Examples of such methods are the classical state-space substructuring (classical-SSS) method [12] and recently the Lagrange multipliers state-space substructuring (LM-SSS) method [25].

The present paper deals with an alternative modal U-K formulation allowing to simplify and optimize the dynamic substructuring of constrained

multibody systems with non-proportional damping, especially in the case of experimental substructuring. The use of complex modes of unconstrained dissipative substructures allows to always obtain a system of uncoupled Ordinary Differential Equations (ODEs) with respect to complex modal coordinates, contrary to existing CMS methods which end up with a fully populated modal damping matrix in case of general viscous damping. Another development is found in the extension of the original U-K formulation to cover the case of vibro-acoustic substructures with an internal cavity. Indeed this type of problem is frequently encountered for example in musical acoustics or practical engineering [26], and the U-K formalism provides an elegant solution expressed in terms of eigenmodes of the unconstrained substructures.

The first section includes a brief recall of the original U-K formulation [5, 9], followed by an extension taking into account vibro-acoustic substructures. Then, the modal domain adaptation developed by Antunes and Debut [20] is touched on as an intermediary step to present the novel modal U-K formulation based on complex modal analysis. In section 3, the validity of this new formulation is assessed through an application to an academic test case with non-proportional damping (also called non-classical damping). Then a practical example, from musical acoustics, based on the combination of analytical and experimental data allows to demonstrate the relevance of this formulation.

2. Udwadia-Kalaba formalism

In order to develop the newly proposed formulation, the original U-K formulation [5–9] is briefly recalled. This allows to introduce an extension

of the latter to subsystems involving internal vibro-acoustic problems. Then the recently developed modal formulation [20] based on modal bases of associated conservative subsystems is briefly covered for completeness. Finally, an alternative modal formulation based on modal bases of under-damped dissipative subsystems is presented and two solutions are proposed depending on the presence/absence of acoustic dofs in the subsystems.

2.1. Physical space

2.1.1. Original formulation

Let $\mathbf{y}_s(t)$ represent the response, and $\mathbf{x}_s(t)$ the degrees of freedom, of a discrete structural mechanical system of mass, damping and stiffness matrices $\mathbf{M}_s$, $\mathbf{C}_s$ and $\mathbf{K}_s$, which consists of J constrained subsystems via constraining forces $\mathbf{f}_c$, subjected to external constraint-independent forces $\mathbf{f}_{\text{nc}}$. The U-K formulation derives from the second order model

$$\begin{gathered}\mathbf{M}_s\ddot{\mathbf{x}}_s(t) + \mathbf{C}_s\dot{\mathbf{x}}_s(t) + \mathbf{K}_s\mathbf{x}_s(t) = \mathbf{D}_s^T\left(\mathbf{f}_{\text{nc}}(\mathbf{x}_s, \dot{\mathbf{x}}_s, t) + \mathbf{f}_{\text{c}}(\mathbf{x}_s, \dot{\mathbf{x}}_s, t)\right) \\ \mathbf{y}_s(t) = \mathbf{D}_s\mathbf{x}_s(t)\end{gathered} \tag{1}$$

with $\mathbf{D}_s$ being the output (or input) shape matrix. While the original formulation was obtained with $\mathbf{D}_s$ being the identity matrix, thus assuming the number of responses equals the number of dofs, it is relevant to develop it for any arbitrary matrix (hence any choice of dofs) thus differentiating system responses and dofs.

Constraining forces can be expressed through Lagrange multipliers [27] λ as

$$\mathbf{f}_{\text{c}} = -\mathbf{A}^T\lambda \tag{2}$$

where $\mathbf{A}(\dot{\mathbf{x}}_s, \mathbf{x}_s, t)$ is the constraint matrix, associated with $\mathbf{b}(\dot{\mathbf{x}}_s, \mathbf{x}_s, t)$ a vector function of the motion, corresponding to the following system of P holo-

nomic and non-holonomic constraints in terms of accelerations

$$\mathbf{A}\ddot{\mathbf{y}}_s = \mathbf{b} \ . \tag{3}$$

By combining Eqs. (1–3), the following augmented differential-algebraic equation (DAE) may be built

$$\begin{bmatrix} \mathbf{M}_s & (\mathbf{A}\mathbf{D}_s)^T \\ \mathbf{A}\mathbf{D}_s & \mathbf{0} \end{bmatrix} \begin{Bmatrix} \ddot{\mathbf{x}}_s \\ \lambda \end{Bmatrix} = \begin{Bmatrix} \mathbf{D}_s^T \mathbf{f}_{\text{nc}} - \mathbf{C}_s \dot{\mathbf{x}}_s - \mathbf{K}_s \mathbf{x}_s \\ \mathbf{b} \end{Bmatrix} \tag{4}$$
$$\mathbf{y}_s = \mathbf{D}_s \mathbf{x}_s.$$

Solving Eq. (4), in the least square sense [28] since $\mathbf{A}$ may be rank deficient, gives the explicit expression of Lagrange multipliers

$$\lambda = -\left(\tilde{\mathbf{A}}\mathbf{M}_s^{-1}\tilde{\mathbf{A}}^T\right)^{\dagger}\left(\mathbf{b} - \tilde{\mathbf{A}}\mathbf{M}_s^{-1}\left(\mathbf{D}_s^T\mathbf{f}_{\text{nc}} - \mathbf{C}_s\dot{\mathbf{x}}_s - \mathbf{K}_s\mathbf{x}_s\right)\right) \text{ where } \tilde{\mathbf{A}} = \mathbf{A}\mathbf{D}_s. \tag{5}$$

Thus, the dynamic response of the constrained system verifies the following differential equation

$$\begin{aligned} \mathbf{M}_s\ddot{\mathbf{x}}_s &= \left(\mathbf{D}_s^T\mathbf{f}_{\text{nc}} - \mathbf{C}_s\dot{\mathbf{x}}_s - \mathbf{K}_s\mathbf{x}_s\right) + \boldsymbol{\Delta}\left(\mathbf{b} - \tilde{\mathbf{A}}\mathbf{M}_s^{-1}\left(\mathbf{D}_s^T\mathbf{f}_{\text{nc}} - \mathbf{C}_s\dot{\mathbf{x}}_s - \mathbf{K}_s\mathbf{x}\right)\right) \\ \mathbf{y}_s &= \mathbf{D}_s\mathbf{x}_s. \end{aligned} \tag{6}$$

with $\boldsymbol{\Delta} = \tilde{\mathbf{A}}^T(\tilde{\mathbf{A}}\mathbf{M}_s^{-1}\tilde{\mathbf{A}}^T)^{\dagger}$. The main result from Udwadia and Kalaba [5, 7] lies in the restatement of Eq. (6), in terms of the unconstrained acceleration $\ddot{\mathbf{x}}_u = \mathbf{M}_s^{-1}\left(\mathbf{D}_s^T\mathbf{f}_{\text{nc}} - \mathbf{C}_s\dot{\mathbf{x}}_s - \mathbf{K}_s\mathbf{x}_s\right)$,

$$\begin{aligned} \ddot{\mathbf{x}}_s &= \ddot{\mathbf{x}}_u + \mathbf{M}_s^{-1/2}\mathbf{B}^{\dagger}(\mathbf{b} - \tilde{\mathbf{A}}\ddot{\mathbf{x}}_u) \\ \mathbf{y}_s &= \mathbf{D}_s\mathbf{x}_s. \end{aligned} \tag{7}$$

with $\mathbf{B}^{\dagger}$ denoting the Moore-Penrose pseudo-inverse of $\mathbf{B} = \tilde{\mathbf{A}}\mathbf{M}_s^{-1/2}$.

2.1.2. Extension to vibro-acoustic substructures

In the case of subsystems involving internal vibro-acoustic problems, assuming lossless fluid-structure interactions, a discrete formulation may be provided by the following matrix system [29]

$$\begin{bmatrix} \mathbf{M}_s & \mathbf{0} \\ \mathbf{L}^T & \mathbf{M}_a \end{bmatrix} \begin{Bmatrix} \ddot{\mathbf{x}}_s \\ \ddot{\mathbf{x}}_a \end{Bmatrix} + \begin{bmatrix} \mathbf{C}_s & \mathbf{0} \\ \mathbf{0} & \mathbf{C}_a \end{bmatrix} \begin{Bmatrix} \dot{\mathbf{x}}_s \\ \dot{\mathbf{x}}_a \end{Bmatrix} + \begin{bmatrix} \mathbf{K}_s & -\mathbf{L} \\ \mathbf{0} & \mathbf{K}_a \end{bmatrix} \begin{Bmatrix} \mathbf{x}_s \\ \mathbf{x}_a \end{Bmatrix} = \begin{bmatrix} \mathbf{D}_s & \mathbf{0} \\ \mathbf{0} & \mathbf{D}_a \end{bmatrix}^T \left(\begin{Bmatrix} \mathbf{f}_s \\ \dot{\mathbf{g}}_a \end{Bmatrix} + \mathbf{f}_{\mathrm{c}} \right)$$
$$\begin{Bmatrix} \mathbf{y}_s \\ \mathbf{y}_a \end{Bmatrix} = \begin{bmatrix} \mathbf{D}_s & \mathbf{0} \\ \mathbf{0} & \mathbf{D}_a \end{bmatrix} \begin{Bmatrix} \mathbf{x}_s \\ \mathbf{x}_a \end{Bmatrix} \tag{8}$$

where $\mathbf{y}_s$ and $\mathbf{y}_a$ are vectors denoting the structural and acoustic responses (at the displacement and pressure levels), $\mathbf{x}_s$ and $\mathbf{x}_a$ represent the structural dofs and the acoustic dofs. The output shape matrix $\mathbf{D}$ is composed of submatrices $\mathbf{D}_s$ and $\mathbf{D}_a$. $\mathbf{M}_s$, $\mathbf{M}_a$, $\mathbf{K}_s$, $\mathbf{K}_a$, $\mathbf{C}_s$ and $\mathbf{C}_a$ are, respectively, the mass, stiffness and damping matrices of the structure and the fluid domain. Note that $\mathbf{M}_a$, $\mathbf{K}_a$ and $\mathbf{C}_a$ are not homogeneous to a mass, a stiffness and a damping but these notations are used by analogy with the solid domain. $\mathbf{L}$ is the vibro-acoustic coupling matrix. $\mathbf{f}_s$ is the vector of external forces applied on the structural components and $\dot{\mathbf{g}}_a$ is associated to acoustic sources in the cavity.

The assembled vectors and matrices of Eq. (8) are defined

$$\mathbf{x}_\star \equiv \begin{Bmatrix} \mathbf{x}_\star^1 \\ \vdots \\ \mathbf{x}_\star^J \end{Bmatrix}, \mathbf{f}_s \equiv \begin{Bmatrix} \mathbf{f}_s^1 \\ \vdots \\ \mathbf{f}_s^J \end{Bmatrix}, \mathbf{g}_a \equiv \begin{Bmatrix} \mathbf{g}_a^1 \\ \vdots \\ \mathbf{g}_a^J \end{Bmatrix}, \mathbf{M}_\star \equiv \mathrm{diag}(\mathbf{M}_\star^1, ..., \mathbf{M}_\star^J) = \begin{bmatrix} \mathbf{M}_\star^1 & & \mathbf{0} \\ & \ddots & \\ \mathbf{0} & & \mathbf{M}_\star^J \end{bmatrix},$$
$$\mathbf{C}_\star \equiv \mathrm{diag}(\mathbf{C}_\star^1, ..., \mathbf{C}_\star^J),\ \mathbf{K}_\star \equiv \mathrm{diag}(\mathbf{K}_\star^1, ..., \mathbf{K}_\star^J),\ \mathbf{L} \equiv \mathrm{diag}(\mathbf{L}^1, ..., \mathbf{L}^J) \tag{9}$$

with $\star$ denoting either s or a.

While Eq. (8) directly expresses the coupling between structural displacement and acoustic pressure, an alternative formulation [30] with a positive definite mass matrix is preferred in the following of this paper

$$\underbrace{\begin{bmatrix}\mathbf{M}_s & \mathbf{0}\\ \mathbf{0} & \mathbf{M}_a\end{bmatrix}}_{\mathbf{M}}\underbrace{\begin{Bmatrix}\ddot{\mathbf{x}}_s\\ \ddot{\mathbf{z}}_a\end{Bmatrix}}_{\ddot{\mathbf{x}}}+\underbrace{\begin{bmatrix}\mathbf{C}_s & -\mathbf{L}\\ \mathbf{L}^T & \mathbf{C}_a\end{bmatrix}}_{\mathbf{C}}\begin{Bmatrix}\dot{\mathbf{x}}_s\\ \dot{\mathbf{z}}_a\end{Bmatrix}+\underbrace{\begin{bmatrix}\mathbf{K}_s & \mathbf{0}\\ \mathbf{0} & \mathbf{K}_a\end{bmatrix}}_{\mathbf{K}}\begin{Bmatrix}\mathbf{x}_s\\ \mathbf{z}_a\end{Bmatrix}=\underbrace{\begin{bmatrix}\mathbf{D}_s & \mathbf{0}\\ \mathbf{0} & \mathbf{D}_a\end{bmatrix}^T}_{\mathbf{D}}\left(\underbrace{\begin{Bmatrix}\mathbf{f}_s\\ \mathbf{f}_a\end{Bmatrix}}_{\mathbf{f}_{\mathrm{nc}}}+\tilde{\mathbf{f}}_{\mathrm{c}}\right)$$
$$\underbrace{\begin{Bmatrix}\mathbf{y}_s\\ \tilde{\mathbf{y}}_a\end{Bmatrix}}_{\mathbf{y}}=\begin{bmatrix}\mathbf{D}_s & \mathbf{0}\\ \mathbf{0} & \mathbf{D}_a\end{bmatrix}\begin{Bmatrix}\mathbf{x}_s\\ \mathbf{z}_a\end{Bmatrix} \tag{10}$$

where $\tilde{\mathbf{y}}_a$ is (up to a multiplicative constant) the acoustic velocity potential such that $\dot{\mathbf{z}}_a = \mathbf{x}_a$ and $\mathbf{f}_a(t) = \mathbf{g}_a(t) - \mathbf{g}_a(0)$.

Assuming that the constraints between vibro-acoustic subsystems may be expressed in the form of Eq. (3) with respect to the response vector $\mathbf{y}$, constraining forces $\tilde{\mathbf{f}}_{\mathrm{c}}$ are expressed as in Eq. (2). Building and solving the augmented DAE of Eq. (4) leads to the differential equation (7) and the result from Udwadia and Kalaba is thus recovered.

While the formulation of Eq. (7) is perfectly valid from a mathematical point of view, in practice it has the disadvantage of requesting the knowledge of physical matrices $\mathbf{M}$, $\mathbf{C}$ and $\mathbf{K}$ and while efficient experimental methods have been developed to estimate mass and stiffness matrices, the experimental estimation of the damping matrix $\mathbf{C}$ remains a difficult task. Moreover, from a computational point of view, the unconstrained acceleration $\ddot{\mathbf{x}}_u$ in

Eq. (7) involves a system of coupled Ordinary Differential Equations (ODE) whose resolution, for subsystems containing a large amount of dofs, might be time consuming. This motivates the use of modal expansion techniques, covered in section 2.2, to transform this system of coupled ODE to an uncoupled one.

2.2. Modal space

2.2.1. Normal modes

In case of subsystems with a classical damping, Antunes & Debut [20] adapted the U-K formulation to continuous flexible system by means of a modal expansion on the modal bases of associated conservative subsystems (principal coordinates). In a similar manner to Eq. (7), they obtained in principal coordinates the following expression for the modal response $\underline{\mathbf{q}}^{\mathrm{p}}$ of the constrained system

$$\begin{aligned} \underline{\ddot{\mathbf{q}}}^{\mathrm{p}} &= \underline{\ddot{\mathbf{q}}}_u^{\mathrm{p}} + (\underline{\mathbf{M}}^{\mathrm{p}})^{-1/2}\underline{\mathbf{B}}^{\dagger}(\mathbf{b} - \underline{\mathbf{A}}\underline{\ddot{\mathbf{q}}}_u^{\mathrm{p}}) \\ \mathbf{y} &= \mathbf{D}\boldsymbol{\Phi}\underline{\mathbf{q}}^{\mathrm{p}} \end{aligned} \tag{11}$$

with $\underline{\mathbf{A}} = \tilde{\mathbf{A}}\boldsymbol{\Phi}$ being the modal constraint matrix and $\underline{\mathbf{B}} = \underline{\mathbf{A}}(\underline{\mathbf{M}}^{\mathrm{p}})^{-1/2}$. $\underline{\ddot{\mathbf{q}}}_u^{\mathrm{p}}$ is the modal acceleration of the unconstrained system governed by the equation

$$\underline{\mathbf{M}}^{\mathrm{p}}\underline{\ddot{\mathbf{q}}}_u^{\mathrm{p}} = \boldsymbol{\Phi}^T\mathbf{D}^T\mathbf{f}_{\mathrm{nc}} - \underline{\mathbf{C}}^{\mathrm{p}}\underline{\dot{\mathbf{q}}}^{\mathrm{p}} - \underline{\mathbf{K}}^{\mathrm{p}}\underline{\mathbf{q}}^{\mathrm{p}} \tag{12}$$

where $\underline{\mathbf{M}}^{\mathrm{p}}$, $\underline{\mathbf{C}}^{\mathrm{p}}$, $\underline{\mathbf{K}}^{\mathrm{p}}$ and $\boldsymbol{\Phi}$ are block diagonal matrices containing, respectively, modal mass, stiffness, damping and shape matrices of all subsystems on their diagonal. As for Eq. 7, Antunes & Debut obtained Eq. 11 with $\mathbf{D}$ equal to the identity matrix, however including this matrix in the formulation explicitly shows it is actually valid for any choice of output shape matrix

as well as if the number of system responses does not match the number of dofs.

2.2.2. Complex modes

If the J subsystems do not verify the assumption of classical damping, the system of equation (12) on unconstrained modal coordinates is non-diagonal which may lead to significant computation time for large subsystems. Apart from computation time considerations, in case of experimental substructuring, the physical damping matrix estimation presents many difficulties which make the use of equation (12) unpractical. The development of another modal formulation based on complex modal analysis (CMA) is thus proposed in this section in order to obtain a diagonal system of unconstrained modal coordinates even for non-proportionally damped substructures, allowing at the same time to shortcut the need for physical damping matrix estimation. At this point it should be emphasized that the use of CMA implies that the J subsystems do not yield rigid body modes.

The usual modal expansion on the basis of modal coordinates of the dissipative system is written

$$\begin{Bmatrix} \mathbf{x} \\ \dot{\mathbf{x}} \end{Bmatrix} = \boldsymbol{\Upsilon}_r \underline{\mathbf{q}} \tag{13}$$

where, for $j = 1, ..., J$ constrained subsystems, the vectors that assemble the corresponding physical responses $\mathbf{x}^j(t)$ and modal responses $\underline{\mathbf{q}}^j(t)$, as well as the matrices that assemble the eigenvalues $\underline{\boldsymbol{\Lambda}}^j$ and the left and right

eigenvectors $\boldsymbol{\Upsilon}_*^j$ (with $*$ being either l or r), are defined

$$\mathbf{x} \equiv \begin{Bmatrix} \mathbf{x}^1 \\ \vdots \\ \mathbf{x}^J \end{Bmatrix}, \underline{\mathbf{q}} \equiv \begin{Bmatrix} \underline{\mathbf{q}}^1 \\ \vdots \\ \underline{\mathbf{q}}^J \end{Bmatrix}, \boldsymbol{\Psi}_* \equiv \begin{bmatrix} \boldsymbol{\Psi}_*^1 & & \mathbf{0} \\ & \ddots & \\ \mathbf{0} & & \boldsymbol{\Psi}_*^J \end{bmatrix}, \underline{\boldsymbol{\Lambda}} \equiv \begin{bmatrix} \underline{\boldsymbol{\Lambda}}^1 & & \mathbf{0} \\ & \ddots & \\ \mathbf{0} & & \underline{\boldsymbol{\Lambda}}^J \end{bmatrix},$$
$$\underline{\mathbf{q}} \equiv \begin{Bmatrix} \underline{\mathbf{q}} \\ \overline{\underline{\mathbf{q}}} \end{Bmatrix}, \boldsymbol{\Psi}_* \equiv \begin{bmatrix} \boldsymbol{\Psi}_* & \overline{\boldsymbol{\Psi}}_* \end{bmatrix}, \underline{\boldsymbol{\Lambda}} \equiv \begin{bmatrix} \underline{\boldsymbol{\Lambda}} & 0 \\ 0 & \overline{\underline{\boldsymbol{\Lambda}}} \end{bmatrix}, \boldsymbol{\Upsilon}_* \equiv \begin{bmatrix} \boldsymbol{\Psi}_* \\ \boldsymbol{\Psi}_* \underline{\boldsymbol{\Lambda}} \end{bmatrix} \tag{14}$$

with, for each subsystem, the modal basis of $2N^j$ unconstrained modes defined at R^j physical coordinates

$$\underline{\mathbf{q}}^j \equiv \begin{Bmatrix} \underline{\mathrm{q}}_1^j \\ \vdots \\ \underline{\mathrm{q}}_{N^j}^j \end{Bmatrix}, \boldsymbol{\Psi}_*^j \equiv \begin{bmatrix} \begin{Bmatrix} \psi_{*,1}^j\left(\vec{r}_1^j\right) \\ \vdots \\ \psi_{*,1}^j\left(\vec{r}_{R^j}^j\right) \end{Bmatrix} \cdots \begin{Bmatrix} \psi_{*,N^j}^j\left(\vec{r}_1^j\right) \\ \vdots \\ \psi_{*,N^j}^j\left(\vec{r}_{R^j}^j\right) \end{Bmatrix} \end{bmatrix}, \underline{\boldsymbol{\Lambda}}^j \equiv \begin{bmatrix} \lambda_1^j & & \mathbf{0} \\ & \ddots & \\ \mathbf{0} & & \lambda_{N^j}^j \end{bmatrix},$$
$$\underline{\mathbf{q}}^j \equiv \begin{Bmatrix} \underline{\mathbf{q}}^j \\ \overline{\underline{\mathbf{q}}}^j \end{Bmatrix}, \boldsymbol{\Psi}_*^j \equiv \begin{bmatrix} \boldsymbol{\Psi}_*^j & \overline{\boldsymbol{\Psi}}_*^j \end{bmatrix}, \underline{\boldsymbol{\Lambda}}^j \equiv \begin{bmatrix} \underline{\boldsymbol{\Lambda}}^j & 0 \\ 0 & \overline{\underline{\boldsymbol{\Lambda}}}^j \end{bmatrix}, \boldsymbol{\Upsilon}_*^j \equiv \begin{bmatrix} \boldsymbol{\Psi}_*^j \\ \boldsymbol{\Psi}_*^j \underline{\boldsymbol{\Lambda}}^j \end{bmatrix}. \tag{15}$$

The total number of pairs of complex conjugate modes is thus $N_{\text{tot}} = \sum_1^J N^j$. It can be shown, following the approach of [31], that left eigenvectors $\boldsymbol{\Psi}_l$ of Eq. (10) are linked to right eigenvectors $\boldsymbol{\Psi}_r$ in the following manner

$$\boldsymbol{\Psi}_r = \begin{Bmatrix} \boldsymbol{\Psi}_s \\ \boldsymbol{\Psi}_a \end{Bmatrix} \text{ then } \boldsymbol{\Psi}_l = \begin{Bmatrix} \boldsymbol{\Psi}_s \\ -\boldsymbol{\Psi}_a \end{Bmatrix} \tag{16}$$

with $\boldsymbol{\Psi}_s$ and $\boldsymbol{\Psi}_a$ corresponding, respectively, to structural and acoustic dofs. In the frame of experimental substructuring, the formulation with respect to displacements and pressures is usually preferred for experimental modal analysis, hence it should be emphasized that right eigenvectors $\tilde{\boldsymbol{\Psi}}_r$ of Eq. (8)

are linked to those of Eq. (10) through the relation

$$\tilde{\boldsymbol{\Psi}}_r = \begin{bmatrix} \boldsymbol{\Psi}_s \\ \boldsymbol{\Psi}_a \underline{\boldsymbol{\Lambda}} \end{bmatrix}. \tag{17}$$

In order to develop the complex modal space version of Eq. (7), Eq. (6) is augmented into a first order state-space model by grouping time derivatives of $\mathbf{x}$ on the left-hand side and associating the identity $\mathbf{M}\dot{\mathbf{x}} = \mathbf{M}\dot{\mathbf{x}}$

$$\begin{gathered} \underbrace{\begin{bmatrix} \mathbf{C} & \mathbf{M} \\ \mathbf{M} & \mathbf{0} \end{bmatrix}}_{\mathbb{U}} \begin{Bmatrix} \dot{\mathbf{x}} \\ \ddot{\mathbf{x}} \end{Bmatrix} - \left(\underbrace{\begin{bmatrix} -\mathbf{K} & \mathbf{0} \\ \mathbf{0} & \mathbf{M} \end{bmatrix}}_{\mathbb{A}} + \begin{bmatrix} \mathbf{ZK} & \mathbf{ZC} \\ \mathbf{0} & \mathbf{0} \end{bmatrix} \right) \begin{Bmatrix} \mathbf{x} \\ \dot{\mathbf{x}} \end{Bmatrix} = \begin{Bmatrix} \left(\mathbb{I}_{N_{\text{dof}}} - \mathbf{Z}\right) \mathbf{D}^T \mathbf{f}_{\text{nc}} + \boldsymbol{\Delta}\mathbf{b} \\ \mathbf{0} \end{Bmatrix} \\ \mathbf{y} = \begin{bmatrix} \mathbf{D} & \mathbf{0} \end{bmatrix} \begin{Bmatrix} \mathbf{x} \\ \dot{\mathbf{x}} \end{Bmatrix} \end{gathered} \tag{18}$$

with $\mathbf{Z} = \boldsymbol{\Delta}\tilde{\mathbf{A}}\mathbf{M}^{-1}$ and $\mathbb{I}_{N_{\text{dof}}}$ the identity matrix of size N_{dof}, the total number of dofs of the subsystems.

The projection of Eq. (18) on the bases of eigen modes of the dissipative unconstrained subsystems leads to

$$\begin{gathered} \underline{\boldsymbol{\Pi}}\dot{\underline{\mathbf{q}}} - \left(\underline{\boldsymbol{\Pi}}\, \underline{\boldsymbol{\Lambda}} + \underbrace{\boldsymbol{\Upsilon}_l^T \begin{bmatrix} \mathbf{ZK} & \mathbf{ZC} \\ \mathbf{0} & \mathbf{0} \end{bmatrix} \boldsymbol{\Upsilon}_r}_{\boldsymbol{\Xi}} \right) \underline{\mathbf{q}} = \underbrace{\boldsymbol{\Upsilon}_l^T \begin{Bmatrix} \left(\mathbb{I}_{N_{\text{dof}}} - \mathbf{Z}\right) \mathbf{D}^T \mathbf{f}_{\text{nc}} + \boldsymbol{\Delta}\mathbf{b} \\ \mathbf{0} \end{Bmatrix}}_{\boldsymbol{\Gamma}} \\ \mathbf{y} = \begin{bmatrix} \mathbf{D} & \mathbf{0} \end{bmatrix} \boldsymbol{\Upsilon}_r \underline{\mathbf{q}} \end{gathered} \tag{19}$$

using the orthogonality properties[1] [33]

$$\boldsymbol{\Upsilon}_l^T \mathbb{U} \boldsymbol{\Upsilon}_r = \boldsymbol{\Psi}_l^T \mathbf{C} \boldsymbol{\Psi}_r + \underline{\boldsymbol{\Lambda}} \boldsymbol{\Psi}_l^T \mathbf{M} \boldsymbol{\Psi}_r + \boldsymbol{\Psi}_l^T \mathbf{M} \boldsymbol{\Psi}_r \underline{\boldsymbol{\Lambda}} = \underline{\boldsymbol{\Pi}},$$
$$\boldsymbol{\Upsilon}_l^T \mathbb{A} \boldsymbol{\Upsilon}_r = -\boldsymbol{\Psi}_l^T \mathbf{K} \boldsymbol{\Psi}_r + \underline{\boldsymbol{\Lambda}} \boldsymbol{\Psi}_l^T \mathbf{M} \boldsymbol{\Psi}_r \underline{\boldsymbol{\Lambda}} = \underline{\boldsymbol{\Pi}}\ \underline{\boldsymbol{\Lambda}}. \tag{20}$$

where $\underline{\boldsymbol{\Pi}}$ is a diagonal matrix characterizing the normalization of complex mode shapes. From Eq. (20), it can be shown that the inverse of the physical mass matrix may be expressed

$$\mathbf{M}^{-1} = \boldsymbol{\Psi}_r \underline{\boldsymbol{\Pi}}^{-1} \underline{\boldsymbol{\Lambda}} \boldsymbol{\Psi}_l^T. \tag{21}$$

The terms $\boldsymbol{\Xi}$ and $\boldsymbol{\Gamma}$ of Eq. (19) may be simplified in the following manner (see Appendix B for more details)

$$\boldsymbol{\Xi} = -\boldsymbol{\Psi}_l^T \boldsymbol{\Delta} \tilde{\mathbf{A}} \boldsymbol{\Psi}_r \underline{\boldsymbol{\Lambda}}^2 \tag{22}$$

$$\text{and} \quad \boldsymbol{\Gamma} = \boldsymbol{\Psi}_l^T \left(\mathbb{I}_{N_{\text{dof}}} - \mathbf{Z} \right) \mathbf{D}^T \mathbf{f}_{\text{nc}} + \boldsymbol{\Psi}_l^T \boldsymbol{\Delta} \mathbf{b}. \tag{23}$$

In the following, two cases are distinguished: first the subsystems are assumed to contain acoustic dofs, a general formulation is obtained for vibro-acoustic subsystems with internal fluid cavities, second the case of subsystems with purely structural dofs is presented and leads to a more compact formulation.

2.2.2.1. Presence of acoustic dofs.

[1] For equivalent expressions in the case of continuous subsystems, the authors recommend the paper by Krenk [32].

Developing $\boldsymbol{\Delta}$ using Eq. (21) and introducing the modal constraint Jacobian matrix $\underline{\mathbf{A}}_* = \left[\underline{\mathbf{A}}_* \quad \overline{\underline{\mathbf{A}}}_*\right] = \tilde{\mathbf{A}}\boldsymbol{\Psi}_*$ ($*$ being either r or l) gives

$$\boldsymbol{\Psi}_l^T \boldsymbol{\Delta} = \underline{\mathbf{A}}_l^T \left(\underline{\mathbf{A}}_r \underline{\boldsymbol{\Pi}}^{-1} \underline{\boldsymbol{\Lambda}} \underline{\mathbf{A}}_l^T\right)^\dagger . \tag{24}$$

and defining now $\underline{\mathbf{B}}_* = \underline{\mathbf{A}}_* \left(\underline{\boldsymbol{\Pi}}^{-1} \underline{\boldsymbol{\Lambda}}\right)^{1/2}$,

$$\boldsymbol{\Psi}_l^T \boldsymbol{\Delta} = \left(\underline{\boldsymbol{\Pi}}^{-1} \underline{\boldsymbol{\Lambda}}\right)^{-1/2} \underline{\mathbf{B}}_l^T \left(\underline{\mathbf{B}}_r \underline{\mathbf{B}}_l^T\right)^\dagger . \tag{25}$$

By left multiplying Eq. (19) by $\underline{\boldsymbol{\Pi}}^{-1}$, the main result finally emerges

$$\begin{aligned} \dot{\underline{\mathbf{q}}} = \left(\mathbb{I}_{2N_{\text{tot}}} - \left(\underline{\boldsymbol{\Pi}}\ \underline{\boldsymbol{\Lambda}}\right)^{-1/2} \underline{\mathbf{B}}_l^T \left(\underline{\mathbf{B}}_r \underline{\mathbf{B}}_l^T\right)^\dagger \underline{\mathbf{A}}_r \underline{\boldsymbol{\Lambda}}\right) \left(\underline{\boldsymbol{\Lambda}} \underline{\mathbf{q}} + \underline{\boldsymbol{\Pi}}^{-1} \boldsymbol{\Psi}_l^T \mathbf{D}^T \mathbf{f}_{\text{nc}}\right) \\ + \left(\underline{\boldsymbol{\Pi}}\ \underline{\boldsymbol{\Lambda}}\right)^{-1/2} \underline{\mathbf{B}}_l^T \left(\underline{\mathbf{B}}_r \underline{\mathbf{B}}_l^T\right)^\dagger \mathbf{b} \\ \mathbf{y} = \begin{bmatrix} \mathbf{D} & \mathbf{0} \end{bmatrix} \boldsymbol{\Upsilon}_r \underline{\mathbf{q}} \end{aligned} \tag{26}$$

which can be restated, in terms of unconstrained modal coordinates governed by $\underline{\boldsymbol{\Pi}} \dot{\underline{\mathbf{q}}}_u = \underline{\boldsymbol{\Pi}}\ \underline{\boldsymbol{\Lambda}} \underline{\mathbf{q}} + \boldsymbol{\Psi}_l^T \mathbf{D}^T \mathbf{f}_{\text{nc}}$, as

$$\begin{aligned} \dot{\underline{\mathbf{q}}} = \dot{\underline{\mathbf{q}}}_u + \left(\underline{\boldsymbol{\Pi}}\ \underline{\boldsymbol{\Lambda}}\right)^{-1/2} \underline{\mathbf{B}}_l^T \left(\underline{\mathbf{B}}_r \underline{\mathbf{B}}_l^T\right)^\dagger \left(\mathbf{b} - \underline{\mathbf{A}}_r \underline{\boldsymbol{\Lambda}} \dot{\underline{\mathbf{q}}}_u\right) \\ \mathbf{y} = \begin{bmatrix} \mathbf{D} & \mathbf{0} \end{bmatrix} \boldsymbol{\Upsilon}_r \underline{\mathbf{q}}. \end{aligned} \tag{27}$$

Eq. (27) thus allows to compute the constrained dynamic response of mechanical systems involving internal vibro-acoustic problems. It should be noted that the validity of this equation stays unchanged in absence of acoustic dofs. However, a more compact form can be expressed in such a case as presented below.

2.2.2.2. Purely structural dofs.

If the subsystems contain only structural dofs, the problem of Eq. (1) is recovered, left and right eigenvectors are thus equal. Similarly to Eq. 21, defining a hermitian modal mass matrix $\underline{\mathbf{M}}$ as $\underline{\mathbf{M}} = \boldsymbol{\Psi}^H \mathbf{M} \boldsymbol{\Psi}$, one obtains

$$\mathbf{M}^{-1} = \boldsymbol{\Psi} \underline{\mathbf{M}}^{-1} \boldsymbol{\Psi}^H. \tag{28}$$

Note that in absence of acoustics dofs the matrix $\underline{\mathbf{M}}$ is semi-definite positive. When performing the complex modal analysis of a structure, the matrix $\underline{\boldsymbol{\Pi}}$ is set by prescribing the normalization of complex mode shapes. As developed in Appendix A the matrix $\underline{\mathbf{M}}$ can then be obtained from $\underline{\boldsymbol{\Pi}}$, assuming $\boldsymbol{\Psi}$ is full column rank (at least as many measured responses as identified pairs of complex modes).

Eq. 24 may be rewritten using Eq. (28) in the following manner

$$\boldsymbol{\Psi}^T \boldsymbol{\Delta} = \underline{\mathbf{A}}^T \left(\underline{\mathbf{A}} \underline{\mathbf{M}}^{-1} \underline{\mathbf{A}}^H \right)^\dagger. \tag{29}$$

Defining now $\underline{\mathbf{E}} = \begin{bmatrix} \underline{\mathbf{E}} & \overline{\underline{\mathbf{E}}} \end{bmatrix} = \underline{\mathbf{A}} \begin{bmatrix} \underline{\mathbf{M}} & 0 \\ 0 & \overline{\underline{\mathbf{M}}} \end{bmatrix}^{-1/2}$ leads to

$$\boldsymbol{\Psi}^T \boldsymbol{\Delta} = \begin{bmatrix} \underline{\mathbf{M}}^{1/2} & 0 \\ 0 & \overline{\underline{\mathbf{M}}}^{1/2} \end{bmatrix}^T \underline{\mathbf{E}}^T \left(\underline{\mathbf{E}} \underline{\mathbf{E}}^H \right)^\dagger = \begin{bmatrix} \overline{\underline{\mathbf{M}}}^{1/2} \overline{\underline{\mathbf{E}}}^\dagger \\ \underline{\mathbf{M}}^{1/2} \underline{\mathbf{E}}^\dagger \end{bmatrix}. \tag{30}$$

By left multiplying Eq. (19) by $\underline{\boldsymbol{\Pi}}^{-1}$, the main result finally emerges

$$\begin{aligned} \dot{\underline{\mathbf{q}}} &= \left(\mathbb{I}_{2N_{\text{tot}}} - \underline{\boldsymbol{\Pi}}^{-1} \begin{bmatrix} \overline{\underline{\mathbf{M}}}^{1/2} \overline{\underline{\mathbf{E}}}^\dagger \\ \underline{\mathbf{M}}^{1/2} \underline{\mathbf{E}}^\dagger \end{bmatrix} \underline{\mathbf{A}} \underline{\boldsymbol{\Lambda}} \right) \left(\underline{\boldsymbol{\Lambda}} \underline{\mathbf{q}} + \underline{\boldsymbol{\Pi}}^{-1} \boldsymbol{\Psi}^T \mathbf{D}^T \mathbf{f}_{\text{nc}} \right) + \underline{\boldsymbol{\Pi}}^{-1} \begin{bmatrix} \overline{\underline{\mathbf{M}}}^{1/2} \overline{\underline{\mathbf{E}}}^\dagger \\ \underline{\mathbf{M}}^{1/2} \underline{\mathbf{E}}^\dagger \end{bmatrix} \mathbf{b} \\ \mathbf{y} &= \begin{bmatrix} \mathbf{D} & \mathbf{0} \end{bmatrix} \boldsymbol{\Upsilon} \underline{\mathbf{q}}. \end{aligned} \tag{31}$$

Thus the constrained response verifies

$$\begin{aligned} \underline{\dot{\mathbf{q}}} &= \underline{\dot{\mathbf{q}}}_u + \underline{\mathbf{\Pi}}^{-1} \begin{bmatrix} \overline{\mathbf{M}}^{1/2} \overline{\mathbf{E}}^{\dagger} \\ \underline{\mathbf{M}}^{1/2} \underline{\mathbf{E}}^{\dagger} \end{bmatrix} \left(\mathbf{b} - \underline{\mathbf{A}\mathbf{\Lambda}} \underline{\dot{\mathbf{q}}}_u \right) \\ \mathbf{y} &= \begin{bmatrix} \mathbf{D} & \mathbf{0} \end{bmatrix} \mathbf{\Upsilon} \underline{\mathbf{q}} \end{aligned} \tag{32}$$

which is equivalent to Eq. (27) in absence of acoustic dofs but more compact. When analyzing the dynamic behavior of multibody systems composed of only structural dofs with non-proportional damping, if the modal mass matrix $\underline{\mathbf{M}}$ is known, the use of Eq. (32) is thus encouraged.

Eqs. (27) and (32) are quite similar to the previously proposed formulations in Eqs. (7) and (11). Indeed, the constrained response is found to be equal to the unconstrained response to which a corrective term, representing the contribution of constraining forces, is added. However, an important difference resides in the order of the obtained system of ODE which was 2 for previous formulations and is now 1. This is a direct consequence of the use of the complex modal space which is made of eigenmodes of the state-space problem of Eq. (18).

To summarize the results of this alternative formulation, and emphasize on the added value with respect to the modal formulation based on real modes, Fig. 1 presents block diagrams of the main steps of the U-K substructuring, for both formulations, as well as those of the experimental modal analysis. It is visible that both formulations involve the same steps: first, input modal parameters of the unconstrained (free interface) substructures as well as constraint-independent forces have to be prescribed, then the response of the subsystems to the constraint-independent forces is computed and finally their constrained response verifying the constraint equations is

determined. In the authors opinion, the main advantage of the formulation proposed in this paper, compared to the one based on real modes, lies in the necessary input modal parameters. Indeed, the experimental estimation of real modes (principal coordinates) of a structure results from the identification of its complex modal basis, mostly by assuming that the structure verifies the hypothesis of proportional damping. Hence, using directly complex modes of the substructures in the U-K formalism removes this step of the experimental modal analysis and avoids resorting to this limiting assumption.

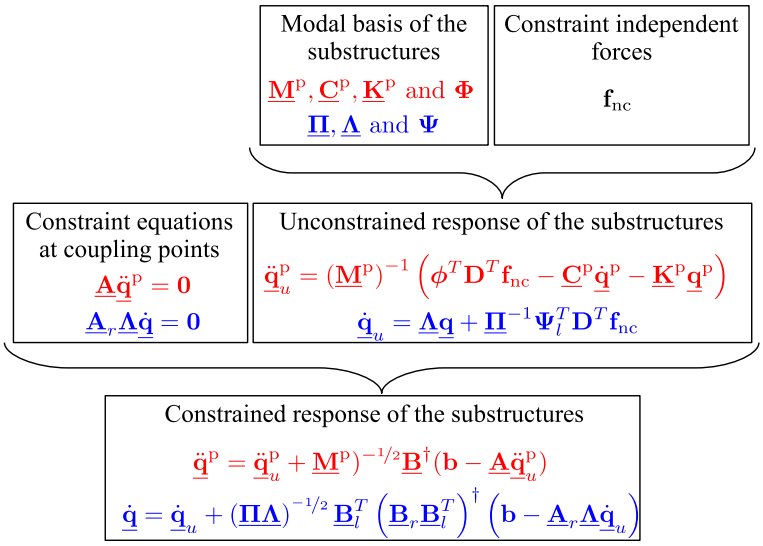

Figure 1: Summary of the UK formalisms based on real modes (red) and complex modes (blue). See sections 2.2.1 and 2.2.2 for details regarding mathematical notations.

3. Application cases

Now that the modal U-K formulation based on complex modes of the dissipative subsystems is developed, its validity is first assessed in the case of a simple academic system. Then two practical examples are presented

and consist in the coupling of the analytical theory of vibrating strings, first, with an experimental 2 dofs fluid-structure guitar model to demonstrate the relevance of this new formulation for internal vibro-acoustic problems, and second, with an experimental 32 dofs structural model of a harp from Central Africa showing high modal complexity.

In order to assess the benefit of taking into account the non-proportionality of the damping, two simulations are compared in all following examples:

Case 1 Truly complex modes of the subsystems are used, leading to a fully populated modal damping matrix $\underline{\mathbf{C}}^P = \mathbf{\Phi}^T \mathbf{C} \mathbf{\Phi}$ in principal coordinates.

Case 2 Falsely complex modes are used to render the modal damping matrix $\underline{\mathbf{C}}^P$ diagonal and equal to $-2\mathrm{Re}(\underline{\mathbf{\Lambda}})$, obtained from the usual approximation[34] of real mode shapes $\tilde{\mathbf{\Phi}} = \mathrm{Re}(\mathbf{\Psi}\sqrt{2\mathrm{jIm}(\underline{\mathbf{\Lambda}})})$ then converted back by $\tilde{\mathbf{\Psi}} = \tilde{\mathbf{\Phi}}/\sqrt{2\mathrm{jIm}(\underline{\mathbf{\Lambda}})}$ with $\mathbf{\Psi}$ normalized such that $\underline{\mathbf{\Pi}}$ is the identity matrix.

Following simulations are obtained using a three-step Adams-Bashforth time integration[35, 36] scheme to solve for complex modal coordinates $\underline{\mathbf{q}}$ from the knowledge of their derivative.

3.1. Academic system

The academic example consists in a 4 dof subsystem S_1 with fixed-free boundary conditions coupled to a 5 dofs subsystem S_2 with free-fixed boundary conditions as depicted in Fig. 2. The coupling constraint is prescribed as a continuity of acceleration between both free ends.

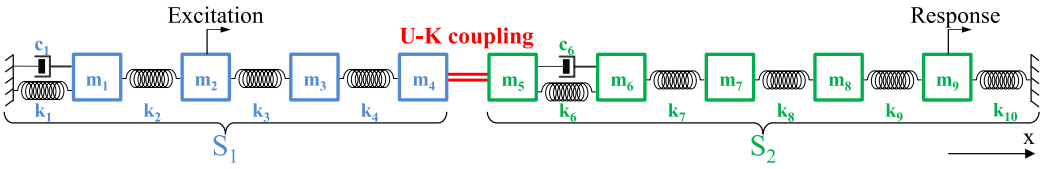

Figure 2: 4 dofs subsystem coupled to 5 dofs subsystem

The global system (after coupling) verifies the following differential equation

$$\mathbf{M}_A\ddot{\mathbf{x}}_A + \mathbf{C}_A\dot{\mathbf{x}}_A + \mathbf{K}_A\mathbf{x}_A = \mathbf{f}_e \tag{33}$$

whose solution in the frequency domain is

$$\tilde{\mathbf{x}}_A = \left(-\omega^2\mathbf{M}_A + \mathrm{j}\omega\mathbf{C}_A + \mathbf{K}_A\right)^{-1}\mathbf{f}_e \tag{34}$$

with $\mathbf{x}_A$ the vector regrouping the displacement of masses [m_1, m_2, m_3, m_4+m_5, m_6, m_7, m_8,m_9] and $\tilde{\mathbf{x}}_A$ its Fourier transform.

Physical matrices of both subsystems are presented in Eqs. (35) and (36). Physical matrices of the global system (after coupling) used in the reference solution are presented in Eq. (37).

$$\mathbf{M}_1 = \begin{bmatrix} 0.1 & 0 & 0 & 0 \\ 0 & 0.2 & 0 & 0 \\ 0 & 0 & 0.2 & 0 \\ 0 & 0 & 0 & 0.1 \end{bmatrix}, \mathbf{K}_1 = \begin{bmatrix} 50 & -30 & 0 & 0 \\ -30 & 70 & -40 & 0 \\ 0 & -40 & 70 & -30 \\ 0 & 0 & -30 & 30 \end{bmatrix}, \mathbf{C}_1 = \begin{bmatrix} 0.5 & 0 & 0 & 0 \\ 0 & 0 & 0 & 0 \\ 0 & 0 & 0 & 0 \\ 0 & 0 & 0 & 0 \end{bmatrix} \quad (35)$$

$$\mathbf{M}_2 = \begin{bmatrix} 0.1 & 0 & 0 & 0 & 0 \\ 0 & 0.1 & 0 & 0 & 0 \\ 0 & 0 & 0.3 & 0 & 0 \\ 0 & 0 & 0 & 0.1 & 0 \\ 0 & 0 & 0 & 0 & 0.2 \end{bmatrix}, \mathbf{K}_2 = \begin{bmatrix} 10 & -10 & 0 & 0 & 0 \\ -10 & 40 & -30 & 0 & 0 \\ 0 & -30 & 40 & -10 & 0 \\ 0 & 0 & -10 & 30 & -20 \\ 0 & 0 & 0 & -20 & 30 \end{bmatrix}, \mathbf{C}_2 = \begin{bmatrix} 0.5 & 0 & 0 & 0 & 0 \\ 0 & 0 & 0 & 0 & 0 \\ 0 & 0 & 0 & 0 & 0 \\ 0 & 0 & 0 & 0 & 0 \\ 0 & 0 & 0 & 0 & 0 \end{bmatrix}$$

(36)

$$\mathbf{M}_A = \begin{bmatrix} \mathbf{M}_1 & \mathbf{0} \\ \mathbf{0} & \mathbf{M}_2 \end{bmatrix}, \mathbf{K}_A = \begin{bmatrix} \mathbf{K}_1 & \mathbf{0} \\ \mathbf{0} & \mathbf{K}_2 \end{bmatrix}, \mathbf{C}_A = \begin{bmatrix} \mathbf{C}_1 & \mathbf{0} \\ \mathbf{0} & \mathbf{C}_2 \end{bmatrix}$$

(37)

The new proposed formulation is used to simulate the dynamic response of the discrete mass m_9 of system S_2 in Fig. 3. A sampling frequency of 4 kHz is used and the full set of complex modes are retained for both subsystems. The excitation consists in an impulse at the initial instant (see the bottom graph of Fig. 3a), applied on the discrete mass m_2 of system S_1, represented by a vector $\mathbf{f}_e[n] = \dfrac{\delta[n]}{dt}$ where dt is the sampling time and $\delta[n]$ is the discrete unit sample function. The waveform of the reference solution in Fig. 3a is obtained by time integration of Eq. 33, using a three-step Adams-Bashforth scheme, and its spectra in Fig. 3b is obtained using Eq. 34.

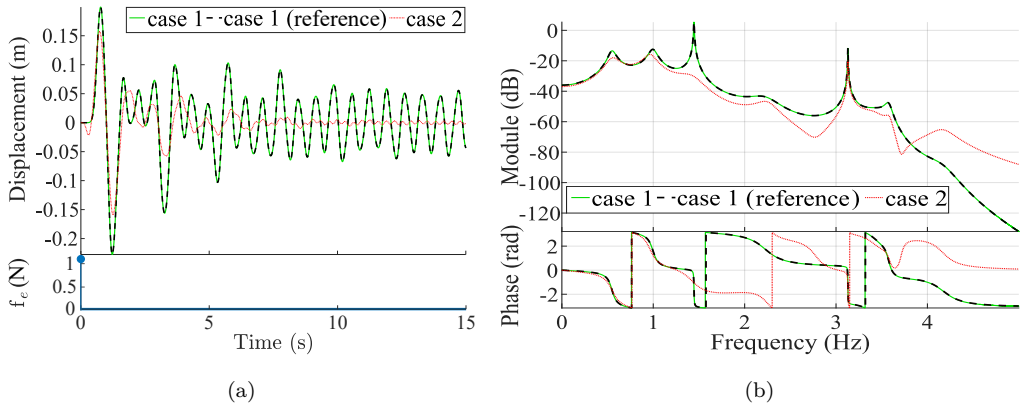

(a) (b)

Figure 3: Simulated displacement waveform and spectrum of the discrete mass m_9 of S_2 for damping cases 1 and 2 together with the reference solution for case 1. (a) waveforms and excitation force, (b) spectra.

First, the complex modal U-K formulation perfectly overlaps with the reference solution when considering the damping case 1 thus validating the inclusion of non-proportional damping. Second, the influence of the proportional damping assumption is clearly visible. Indeed, the simulation relying on the assumption of proportional damping presents globally lower resonance amplitudes. More importantly, the third mode at 1.45 Hz appears to be much more damped than it really is in the reference solution. These differences come from the fact that the modal bases of S_1 and S_2 contain truly complex modes (not proportional to modes of the conservative subsystems up to a complex multiplicative constant) as visible on Figs. (4a-4b) and indicated by the Modal Phase Colinearity [37, 38] (MPC) in Tab. 1, corresponding to the Modal Assurance Criterion [39, 40] (MAC) between a mode shape and its complex conjugate

$$\mathrm{MPC}(\mathbf{u}) = \mathrm{MAC}(\mathbf{u}, \overline{\mathbf{u}}) = \left(\frac{|\mathbf{u}^H \overline{\mathbf{u}}|}{||\mathbf{u}||\ ||\overline{\mathbf{u}}||} \right)^2 .$$

Thus the dynamic responses of S_1 and S_2 cannot be exactly represented by a set of uncoupled equations in principal coordinates.

f_n (Hz)	0.71	2.48	3.66	4.21
MPC	1.00	0.97	0.85	0.69

(a)

f_n (Hz)	0.42	1.33	1.61	3.13	3.59
MPC	0.98	0.66	0.42	1.00	0.99

(b)

Table 1: Modal phase colinearity criteria of S_1 and S_2 for the damping case 1. (a) subsystem S_1, (b) subsystem S_2.

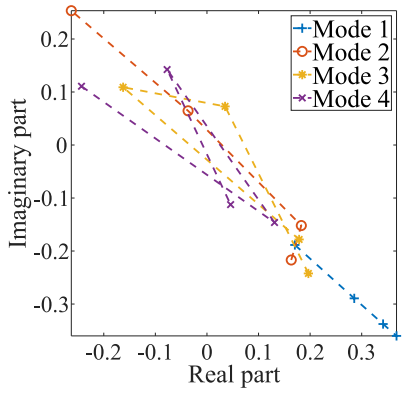

(a)

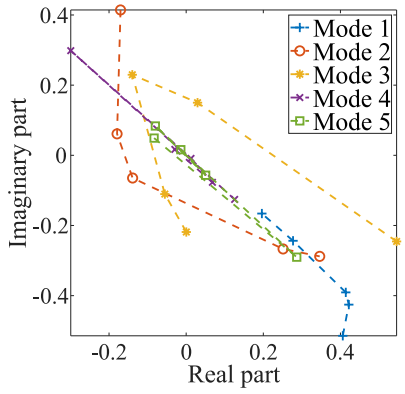

(b)

Figure 4: Complex mode shapes of S_1 and S_2 for the damping case 1. (a) subsystem S_1, (b) subsystem S_2.

3.2. Experimental data

3.2.1. Guitar model

As a second example of application, a free-fixed stiff string is coupled to a 2 dofs guitar model, experimentally identified in [41]. The 2 dofs corre-

spond respectively to the structural transverse displacement of a point on the soundboard, and the acoustic pressure in the middle of the sound hole. Physical mass, damping and stiffness matrices corresponding to the matrix formulation of Eq. (10) (using Eq. (8 - 9)) are

$$\mathbf{M} = \begin{bmatrix} 0.031 & 0 \\ 0 & 2.7 \cdot 10^{-7} \end{bmatrix}, \mathbf{K} = \begin{bmatrix} 2.2 \cdot 10^{4} & 0 \\ 0 & 0.12 \end{bmatrix}, \mathbf{C} = \begin{bmatrix} 1.4 & -0.036 \\ 0.036 & 3.1 \cdot 10^{-6} \end{bmatrix}. \tag{38}$$

Note that physical matrices of Eq. 38 could be prescribed on a theoretical basis, however the choice is made to use experimental data to ensure their order of magnitude.

Following simulations are obtained using a sampling frequency of 1200 kHz and a ramp of force of 1 s, with a maximum amplitude of 1.1 N, applied on the string at three-fifths of its length, represented by a vector $\mathbf{f}_e[n] = \left(H[n] - H\left[n - \frac{1}{dt}\right]\right) 1.1\ n\ dt$ with $H[n]$ being the Heaviside step function (see the bottom graph of Fig. 5a). The string has a radius of 0.48 mm, a length of 64 cm, a density of 1100 kg m^{-3}, a Young's modulus of 7.4 GPa and a tuning frequency of 82.4 Hz. Its transverse displacement is described by 150 modes.

Fig. 5 presents the dynamic response of the structural dof of the guitar model in terms of waveform and spectrum for the damping cases 1 and 2. The MPCs of the two vibro-acoustic complex modes of the system described by physical matrices of Eq. (38) are equal to 1, therefore there mode shapes are proportional to the eigenvectors of the associated conservative system. This means that the latter are orthogonal to the damping matrix $\mathbf{C}$ and no difference should be visible between damping cases 1 and 2. Indeed, the two

362 simulations perfectly overlap in Figs. 5a - 5c which confirms the assumption
363 of proportional damping for this system.

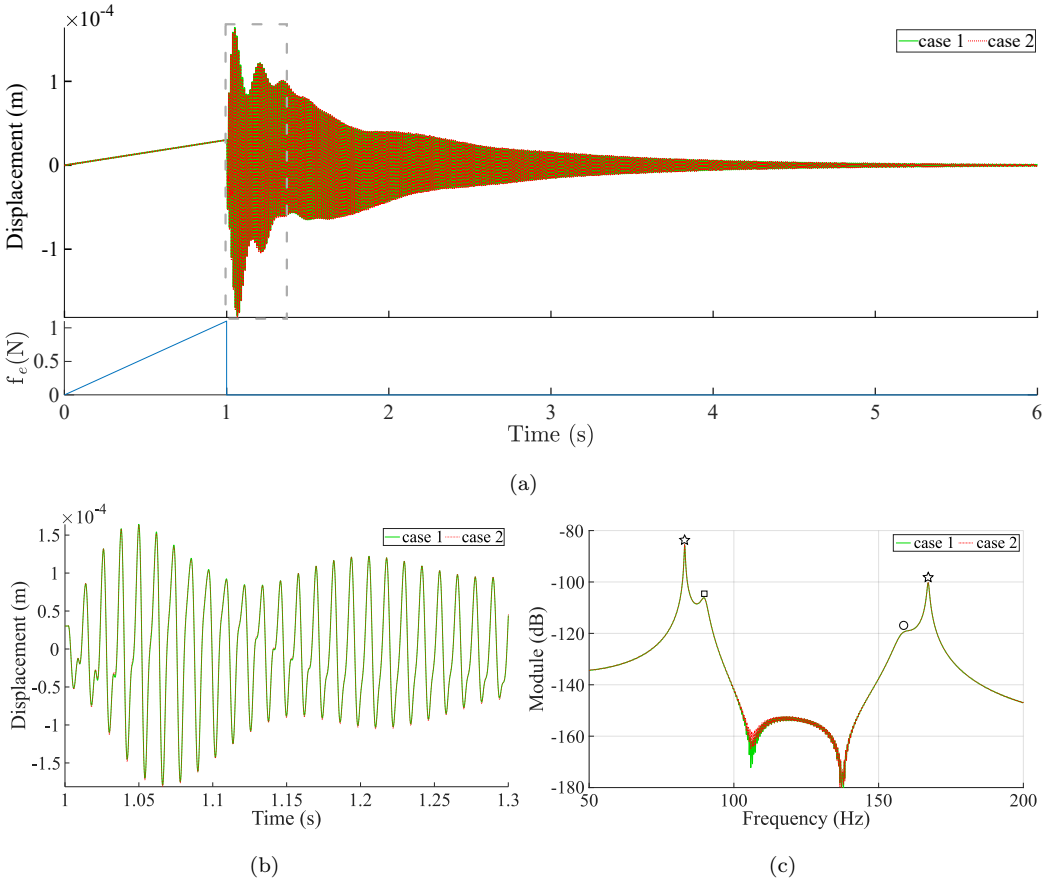

Figure 5: Simulated displacement waveform and spectrum of the structural dof of the guitar for damping cases 1 and 2. (a) waveforms and excitation force, (b) zoom on waveforms in the time frame [1 - 1.3] s, (c) spectra (stars indicate string partials, the square indicates the air cavity resonance inside the soundbox and the circle indicates the soundboard resonance).

3.2.2. Central Africa harp model

As a last example, experimentally identified modal parameters of a harp from Central Africa, in the frequency range [100-1700] Hz, are used to demonstrate the interest of including the non-proportionality of the damping. Indeed, the making process of this harp is artisanal and involves natural materials such as animal skin (for the soundboard). It is thus probable for such materials that the assumption of a uniformly distributed damping is not verified.

The experimental setup, presented in Fig. 6, consists in the harp hanging by means of bungee cords to approximate free boundary conditions. A strip of felt is intertwined with the strings to dampen, at least, their transverse vibrations. Frequency Response Functions are then obtained using a roving automatic hammer (force sensor PCB 086E80) at string attachments points on the neck (in two perpendicular directions) and the tailpiece for three reference positions (accelerometers: PCB M352C65 and 356A03 (triaxial)) placed at the 5^{th} string/neck attachment point and at the 7^{th} string/tailpiece attachment point.

The MPCs of the 32 experimentally estimated complex modes (see Fig. 7a) show that several modes cannot be approximated by real ones and are actually strongly coupled either by damping or frequency. To illustrate this, Fig. 7b shows the separation criterion proposed by Hasselman [42] to characterize the decoupling between modes

$$\frac{2\xi_j\omega_j}{|\omega_j - \omega_k|} \ll 1 \tag{39}$$

with ξ_j the loss factor of mode j, ω_j and ω_k the undamped natural frequencies of modes j and k. This criterion signifies that the coupling due

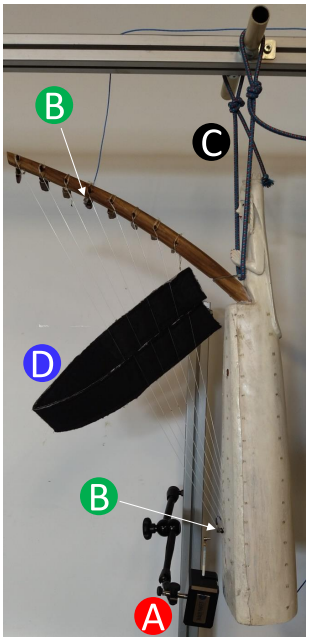

Figure 6: Experimental setup used for the modal analysis of the harp. Ⓐ: Automatic hammer; Ⓑ: Accelerometers; Ⓒ: Bungee cord; Ⓓ: Strip of felt.

to non-proportional damping can be neglected if the cross-modal impedance is high. As suggested by Balmès [33], this criterion can be used to identify groups of modes verifying the assumption of block proportional damping and then, for each group, a proper basis is approximated by resolution of an algebraic Riccati equation [43]. For example, Fig. 7c shows mode combinations (colored in black) for which this criterion crosses the threshold of 0.2 as well as four groups of modes (red dashed squares) whose coupling by damping can be considered rather negligible.

Fig. 8 presents simulations of waveforms and spectra of the acceleration of the 4^{th} string/tailpiece coupling point for damping cases 1 and 2. The simulations are obtained using a sampling frequency of 800 kHz and a ramp

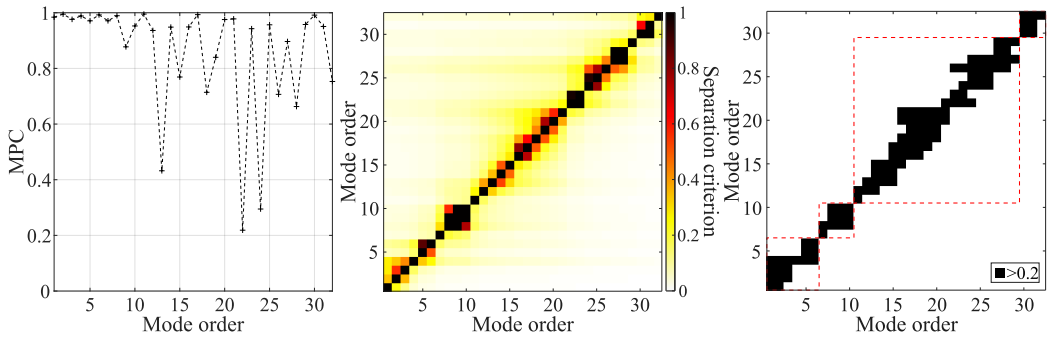

Figure 7: Mode complexity and coupling quantification of experimental modal basis. (a) Modal Phase Colinearity (b) Separation criterion of Eq. (39), (c) Binarized separation criterion with a threshold of 0.2 (red dashed squares indicate uncoupled groups of modes).

of force of 1 s, with a maximum amplitude of 1.1 N, applied on the string at three-fifths of its length (as in section 3.2.1). The string has a radius of 0.4 mm, a length of 52.3 cm, a density of 1100 kg m^{-3}, a Young's modulus of 7.4 GPa and a tuning frequency of 247 Hz. It makes an angle of 23.6 ° with the soundboard and its transverse displacement is described by 150 modes.

Noticeable differences appear on waveforms of Fig. 8a between the proportionally and non-proportionally damped models. Looking at the frequency domain representation on Fig. 8b, two explanations are found. Firstly, amplitude differences are visible in the vicinity of harp body modes responding at the string attachment point and whose MPC is below 0.95 (indicated by colored circles placed above the curves) showing that neglecting the damping coupling between mode combinations not verifying the separation criterion of Eq. (39) leads to an erroneous dynamic response of the system. Secondly, and most importantly, the 3^{rd} and 4^{th} string partials almost coincide with two strongly complex body modes of the non-proportionally damped system

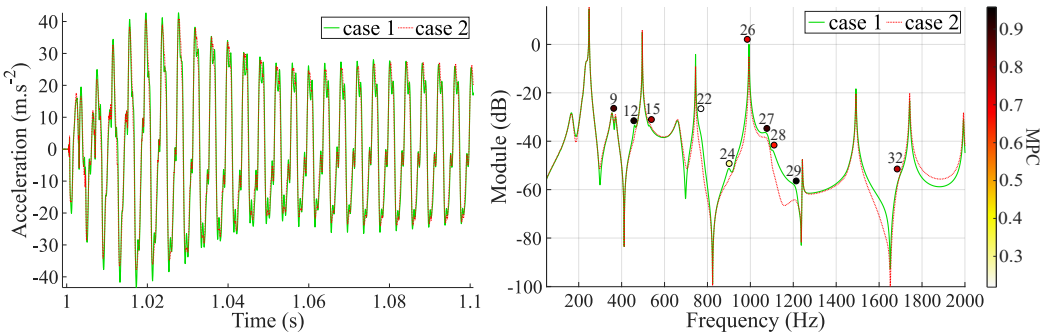

(a) (b)

Figure 8: Simulated acceleration waveform and spectrum of the 4^{th} string/tailpiece coupling point on a harp from Central Africa for damping cases 1 and 2. Colored circles indicate resonances of the harp body around which case 1 and case 2 show significant amplitude differences, numbers indicate mode orders corresponding to Fig. 7. (a) waveforms, (b) spectra.

(n°22 and 26) and are thus underestimated, due to previously mentioned reasons, by approximately 2 to 5 dB in the damping case 2.

4. Conclusion

An alternative modal Udwadia-Kalaba formulation based on complex modes of the dissipative subsystems is proposed. This new formulation is developed in the general case of vibro-acoustic substructures with an internal cavity, to which purely structural substructures previously addressed in the literature is just a particular case. This new formulation is of particular interest in the frame of experimental substructuring, where physical damping matrices of substructures are usually not well estimated, since only a diagonal first order model based on eigenvectors of the state-space representation of each subsystem is required instead of a second order model relying on a po-

tentially fully populated modal damping matrix in case of non-proportional damping. Moreover, the assumption of proportional damping is expected to be less and less reasonable with the increase of modal density so that the modal damping matrix should be more and more populated with the increase of frequency, as long as a modal description of the substructures remains consistent.

The new formulation developed in this paper is validated by comparing simulations of two coupled 4 and 5 dofs subsystems to the analytic solution of an equivalent academic 8 dofs system. Then an application based on the coupling of a string to an experimental vibro-acoustic guitar body model illustrates the advantage of adapting the Udwadia-Kalaba formulation to this type of problem. Finally, experimentally identified complex modes of a harp from Central Africa are coupled to a string in order to show the relevance of using a formulation directly based on complex modes of subsystems instead of relying on real modes usually obtained by assuming a proportional damping.

Acknowledgement

This work, part of the project Ngombi, was funded by the Agence Nationale de la Recherche (French National research agency), Grant No. ANR-19-CE27-0013-01.

Appendix A. Inverse of the modal mass matrix

In the case of experimentally identified modal parameters, the physical mass matrix $\mathbf{M}$ may be unknown and a direct expression of the modal mass

matrix $\underline{\mathbf{M}}$ in term of the norm matrix of complex mode shapes $\underline{\mathbf{\Pi}}$ would be useful.

Both $\underline{\mathbf{M}}$ and $\underline{\mathbf{\Pi}}$ can be linked to $\mathbf{M}$ as

$$\mathbf{M}^{-1} = \mathbf{\Psi}\underline{\mathbf{M}}^{-1}\mathbf{\Psi}^H \text{ and } \mathbf{M}^{-1} = \mathbf{\Psi}\underline{\mathbf{\Pi}}^{-1}\underline{\mathbf{\Lambda}}\mathbf{\Psi}^T \tag{A.1}$$

Since $\mathbf{\Psi}$ is full column rank , the following property is verified

$$\mathbf{\Psi}^\dagger\mathbf{\Psi} = \mathbb{I}_{N_{\text{tot}}} \text{ with } \mathbf{\Psi}^\dagger = \left(\mathbf{\Psi}^H\mathbf{\Psi}\right)^{-1}\mathbf{\Psi}^H. \tag{A.2}$$

Thus

$$\mathbf{\Psi}^\dagger\mathbf{\Psi}\underline{\mathbf{M}}^{-1}\mathbf{\Psi}^H\left(\mathbf{\Psi}^\dagger\right)^H = \underline{\mathbf{M}}^{-1} \tag{A.3}$$

Finally

$$\underline{\mathbf{M}}^{-1} = \mathbf{\Psi}^\dagger\mathbf{\Psi}\underline{\mathbf{\Pi}}^{-1}\underline{\mathbf{\Lambda}}\mathbf{\Psi}^T\left(\mathbf{\Psi}^\dagger\right)^H = \left[\mathbb{I}_{N_{\text{tot}}} \quad \mathbf{\Psi}^\dagger\overline{\mathbf{\Psi}}\right]\underline{\mathbf{\Pi}}^{-1}\underline{\mathbf{\Lambda}}\begin{bmatrix}\left(\overline{\mathbf{\Psi}}^\dagger\mathbf{\Psi}\right)^T \\ \mathbb{I}_{N_{\text{tot}}}\end{bmatrix} \tag{A.4}$$

Appendix B. Development of $\mathbf{\Xi}$

$$\mathbf{\Xi} = \mathbf{\Psi}^T\mathbf{\Delta}\mathbf{A}\mathbf{M}^{-1}\mathbf{K}\mathbf{\Psi} + \mathbf{\Psi}^T\mathbf{\Delta}\mathbf{A}\mathbf{M}^{-1}\mathbf{C}\mathbf{\Psi}\underline{\mathbf{\Lambda}} \tag{B.1}$$

$$= \mathbf{\Psi}^T\mathbf{\Delta}\mathbf{A}\mathbf{M}^{-1}\left(\mathbf{K}\mathbf{\Psi} + \mathbf{C}\mathbf{\Psi}\underline{\mathbf{\Lambda}}\right) \qquad \text{with } \mathbf{M}^{-1} = \mathbf{\Psi}\underline{\mathbf{\Pi}}^{-1}\underline{\mathbf{\Lambda}}\mathbf{\Psi}^T \text{ [33]} \tag{B.2}$$

$$= \mathbf{\Psi}^T\mathbf{\Delta}\mathbf{A}\mathbf{\Psi}\underline{\mathbf{\Pi}}^{-1}\underline{\mathbf{\Lambda}}\left(\mathbf{\Psi}^T\mathbf{K}\mathbf{\Psi} + \mathbf{\Psi}^T\mathbf{C}\mathbf{\Psi}\underline{\mathbf{\Lambda}}\right) \tag{B.3}$$

$$= -\mathbf{\Psi}^T\mathbf{\Delta}\mathbf{A}\mathbf{\Psi}\underline{\mathbf{\Pi}}^{-1}\underline{\mathbf{\Lambda}}\mathbf{\Psi}^T\mathbf{M}\mathbf{\Psi}\underline{\mathbf{\Lambda}}^2 \qquad \text{from Eq. (20)} \tag{B.4}$$

$$= -\mathbf{\Psi}^T\mathbf{\Delta}\mathbf{A}\mathbf{\Psi}\underline{\mathbf{\Lambda}}^2. \tag{B.5}$$

References

[1] D. de Klerk, D.J. Rixen, S.N. Voormeeren, General Framework for Dynamic Substructuring: History, Review and Classification of Techniques, AIAA Journal. 46 (2008) 1169–1181. https://doi.org/10.2514/1.33274.

[2] A. Laulusa, O.A. Bauchau, Review of Classical Approaches for Constraint Enforcement in Multibody Systems, J. Comput. Nonlinear Dyn. 3 (2007) 011004. https://doi.org/10.1115/1.2803257.

[3] G.A. Maggi, Principii della teoria matematica del movimento dei corpi: corso di meccanica razionale [Principles of the mathematical theory of the motion of bodies: a course in rational mechanics], U. Hoepli, Milano, 1896.

[4] J.I. Neĭmark, N.A. Fufaev, Dynamics of nonholonomic systems, Amer. Math. Soc., Providence, RI, 1972.

[5] F.E. Udwadia, R.E. Kalaba, A new perspective on constrained motion, Proc. R. Soc. Lond. A. 439 (1992) 407–410. https://doi.org/10.1098/rspa.1992.0158.

[6] F.E. Udwadia, R.E. Kalaba, The Geometry of Constrained Motion, Z. Angew. Math. Mech. 75 (1995) 637–640. https://doi.org/10.1002/zamm.19950750823.

[7] F.E. Udwadia, Equations of motion for mechanical systems: A unified approach, Int. J. Non-Linear Mech. 31 (1996) 951–958. https://doi.org/10.1016/S0020-7462(96)00116-3.

[8] F.E. Udwadia, R.E. Kalaba, What is the General Form of the Explicit Equations of Motion for Constrained Mechanical Systems?, J. Appl. Mech. 69 (2002) 335–339. https://doi.org/10.1115/1.1459071.

[9] A. Arabyan, F. Wu, An Improved Formulation for Constrained Mechanical Systems, Multibody Sys. Dyn. 2 (1998) 49–69. https://doi.org/10.1023/A:1009724704839.

[10] S. Bi, M. Beer, M. Ouisse, E. Foltête, Identification of system matrices based on experimental modal analysis and its application in structural health monitoring, in: Proceedings of the 13th International Conference on Applications of Statistics and Probability in Civil Engineering, ICASP 2019, KOR, 2019. https://strathprints.strath.ac.uk/79627/.

[11] B. Jetmundsen, R.L. Bielawa, W.G. Flannelly, Generalized Frequency Domain Substructure Synthesis, J. Am. Helicopter Soc. 33 (1988) 55–64. https://doi.org/10.4050/JAHS.33.1.55.

[12] T.-J. Su, J.-N. Juang, Substructure system identification and synthesis, J. Guid. Control Dyn. 17 (1994) 1087–1095. https://doi.org/10.2514/3.21314.

[13] M. Imregun, D.A. Robb, Structural modification via FRF coupling using measured data, in: Proceedings of the 10th International Modal Analysis Conference, Society for Experimental Mechanics, Bethel, CT, 1992: pp. 1095–1099.

[14] J.R. Crowley, A.L. Klosterman, G.T. Rocklin, H. Vold, Direct structural

modification using frequency response functions, Proceedings of the 2nd International Modal Analysis Conference (IMAC II). (1984) 58–65.

[15] D. de Klerk, D.J. Rixen, J. de Jong, The frequency based substructuring (FBS) method reformulated according to the dual domain decomposition method, in: Proceedings of the XXIV International Modal Analysis Conference, (IMAC XXIV), Society for Experimental Mechanics, Bethel, CT, St Louis, MO, 2006: pp. 1–14.

[16] R. Craig, Jr., Coupling of substructures for dynamic analyses - An overview, in: Proceedings of the 41st Structures, Structural Dynamics, and Materials Conference, AIAA/ASME/ASCE/AHS/ASC, Atlanta,GA,U.S.A., 2000. https://doi.org/10.2514/6.2000-1573.

[17] R.R. Craig, M.C.C. Bampton, Coupling of substructures for dynamic analyses., AIAA Journal. 6 (1968) 1313–1319. https://doi.org/10.2514/3.4741.

[18] R.H. MacNeal, A hybrid method of component mode synthesis, Comput. Struct. 1 (1971) 581–601. https://doi.org/10.1016/0045-7949(71)90031-9.

[19] S. Rubin, Improved Component-Mode Representation for Structural Dynamic Analysis, AIAA Journal. 13 (1975) 995–1006. https://doi.org/10.2514/3.60497.

[20] J. Antunes, V. Debut, Dynamical computation of constrained flexible systems using a modal Udwadia-Kalaba formulation: Applica-

tion to musical instruments, J. Acoust. Soc. Am. 141 (2017) 764–778. https://doi.org/10.1121/1.4973534.

[21] V. Debut, J. Antunes, Physical synthesis of six-string guitar plucks using the Udwadia-Kalaba modal formulation, J. Acoust. Soc. Am. 148 (2020) 575–587. https://doi.org/10.1121/10.0001635.

[22] J.-T. Jiolat, C. d'Alessandro, J.-L. Le Carrou, J. Antunes, Toward a physical model of the clavichord, J. Acoust. Soc. Am. 150 (2021) 2350–2363.

[23] J.-T. Jiolat, J.-L. Le Carrou, C. d'Alessandro, Whistling in the clavichord, J. Acoust. Soc. Am. 153 (2023) 338–347. https://doi.org/10.1121/10.0016825.

[24] J. Antunes, V. Debut, L. Borsoi, X. Delaune, P. Piteau, A modal Udwadia-Kalaba formulation for vibro-impact modelling of continuous flexible systems with intermittent contacts, Procedia Engineering. 199 (2017) 322–329. https://doi.org/10.1016/j.proeng.2017.09.058.

[25] R.S.O. Dias, M. Martarelli, P. Chiariotti, Lagrange Multiplier State-Space Substructuring, J. Phys. Conf. Ser. 2041 (2021) 012016. https://doi.org/10.1088/1742-6596/2041/1/012016.

[26] M. Maess, L. Gaul, Substructuring and model reduction of pipe components interacting with acoustic fluids, Mech. Syst. and Signal Process. 20 (2006) 45–64. https://doi.org/10.1016/j.ymssp.2005.02.008.

[27] A.A. Shabana, Forms of the dynamic equations, in: Computational Dynamics, John Wiley & Sons, Ltd, 2010: pp. 177–210. https://doi.org/10.1002/9780470686850.ch4.

[28] D. de Falco, E. Pennestrì, L. Vita, Investigation of the Influence of Pseudoinverse Matrix Calculations on Multibody Dynamics Simulations by Means of the Udwadia-Kalaba Formulation, J. Aerosp. Eng. 22 (2009) 365–372. https://doi.org/10.1061/(ASCE)0893-1321(2009)22:4(365).

[29] H.J.-P. Morand, R. Ohayon, Fluid structure interaction-Applied numerical methods, J. Wiley and Sons, Chichester, 1995.

[30] G.C. Everstine, A symmetric potential formulation for fluid-structure interaction, Journal of Sound and Vibration 79 (1981) 157–160. https://doi.org/10.1016/0022-460X(81)90335-7.

[31] K. Wyckaert, F. Augusztinovicz, P. Sas, Vibro-acoustical modal analysis: Reciprocity, model symmetry, and model validity, J. Acoust. Soc. Am. 100 (1998) 3172–3181. https://doi.org/10.1121/1.417127.

[32] S. Krenk, Complex modes and frequencies in damped structural vibrations, J. Sound Vib. 270 (2004) 981–996. https://doi.org/10.1016/S0022-460X(03)00768-5.

[33] E. Balmés, New results on the identification of normal modes from experimental complex modes, Mech. Syst. Signal Process. 11 (1997) 229–243. https://doi.org/10.1006/mssp.1996.0058.

[34] J. Piranda, Analyse modale expérimentale [Experimental modal analysis], Techniques de l'ingénieur RD2 (2001) 1–29.

[35] F. Bashforth, J.C. Adams, An Attempt to Test the Theories of Capillary Action by Comparing the Theoretical and Measured Forms of Drops of Fluid, Cambridge University Press, London, 1883.

[36] J.C. Butcher, Numerical methods for ordinary differential equations in the 20th century, J. Comput. Appl. Math. 125 (2000) 1–29. https://doi.org/10.1016/S0377-0427(00)00455-6.

[37] R.S. Pappa, K.B. Elliott, A. Schenk, Consistent-mode indicator for the eigensystem realization algorithm, J. Guid. Control Dyn. 16 (1993) 852–858. https://doi.org/10.2514/3.21092.

[38] P. Vacher, B. Jacquier, A. Bucharles, Extensions of the MAC criterion to complex modes, in: Proceedings of the International Conference on Noise and Vibration Engineering (ISMA), Leuven, Belgium, 2010: pp. 2713–2726.

[39] R.J. Allemang, Investigation of some multiple input/output frequency response function experimental modal analysis techniques, Doctor of Philosophy Dissertation, University of Cincinnati, Mechanical Engineering Department, 1980.

[40] R.J. Allemang, A Correlation Coefficient for Modal Vector Analysis, in: Proceedings of the 1st International Modal Analysis Conference, 1982: pp. 110–116.

[41] E. Foltete, M. Ouisse, J.-L. Le Carrou, F. Gauthier, Analyse modale expérimentale de systèmes vibroacoustiques : application aux modes A0 et T1 de la guitare et de la harpe [Experimental modal analysis

of vibroacoustic systems: application to the A0 and T1 modes of the guitar and harp], in: 8ème Congrès Français d'Acoustique (CFA'06), Tours, France, 2006: pp. 577–580. https://hal.science/hal-00178384.

[42] T.K. Hasselman, Modal coupling in lightly damped structures, AIAA Journal. 14 (1976) 1627–1628. https://doi.org/10.2514/3.7259.

[43] D. Bini, B. Iannazzo, B. Meini, Numerical solution of algebraic Riccati equations, SIAM, Philadelphia, 2011.